 https://doi.org/10.3311/PPee.21047

Periodica Polytechnica Electrical Engineering and Computer Science, 67(2), pp. 136–148, 2023

Multilevel Converter and Fuzzy Logic Solutions for Improving Direct Control Accuracy of DFIG-based Wind Energy System

Oualid Djoudi[1*], Sofia Lalouni Belaid[1], Salah Tamalouzt[1]

[1] Laboratoire de Technologie Industrielle et de l'Information (LTII), Faculté de Technologie, Université de Bejaia, 06000 Bejaia, Algeria
[*] Corresponding author, e-mail: oualid.djoudi@univ-bejaia.dz

Received: 22 August 2022, Accepted: 16 January 2023, Published online: 21 March 2023

Abstract

The purpose of this study is to enhance the accuracy of direct power/torque control (DPC/DTC) applied to back-to-back converters supplying a doubly fed induction generator (DFIG) based wind power system. Two solutions are proposed. The first one is to increase the degree of freedom of the DTC and DPC control by implementing three-level back-to-back converters. Fuzzy logic control is the second solution to enhance the performances of both conventional direct power/torque control, leading in a decrease of the DFIG's torque/flux ripples and the active/reactive powers ripples supplied by the grid side converter, consequently, reduce the grid currents' total harmonic distortion (THD). The MATLAB/Simulink environment is used to evaluate the wind power generation system performances. The collected findings show that the fuzzy direct control (FDC) technique outperforms conventional direct control (CDC) when used for two-level back-to-back converters.

Keywords

doubly fed induction generator, conventional direct control, three-level converters, fuzzy direct control, wind energy system

1 Introduction

Wind turbine (WT) is quickly becoming a favorite renewable power source, thanks to a set of merits, such as availability and eco-friendly nature. The wind energy conversion system (WECS) allows reducing greenhouse gas emissions [1–3]. The WECS based on a doubly fed induction generator (DFIG) is now the most frequently utilized in wind farms; it can operate in different modes with variable and wide speed range. Since low power converters are used on the rotor side, the power losses are minimized [4, 5]. The DFIG's rotor side control is characterized by controlling two back-to-back converters. The grid-side converter (GSC) manages the DC-link voltage and reactive power of the given rotor, while the rotor-side converter (RSC) regulates the generated active and reactive powers [6, 7].

Vector-oriented control (VOC) is the conventional method used to control DFIG, using proportional integral (PI) regulators [8, 9]. This approach offers good statistics through the presence of an internal current loop, and low powers ripples transited to the grid [10]. However, it presents a slow transient response and is sensitive to the system's parametric variations, qualified as a non-robust method, which limits its use [11]. The direct control (DC) technique is an alternative to the VOC. A direct torque control (DTC) directly regulates the DFIG rotor flux and the electromagnetic torque. On the other hand, direct power control (DPC) system is designed to directly track the grid's active/reactive powers references.

The DTC can be easily set up because there is no pulse width modulation (PWM) block, and it is robust to the parametric variations [7]. However, this control suffers from the ripples generated by a variable switching frequency and switching losses caused by hysteresis controllers. In [12], a comparison of VOC and DTC applied to doubly fed induction motor is performed and a slow transient response is observed with VOC. Moreover, the torque ripples are more important with DTC.

Several approaches have recently been taken to increase the DC performances. They are applied to the two-level (2L) back-to-back converter in the DFIG by incorporating other techniques [13]. For the GSC control, several methods have been tested to reduce the variation of the DPC switching frequency [14–16]. In [14], a new DPC technique is proposed. This one doesn't require the use of phase-locked loop (PLL) and Park transforms for active/reactive powers control. It is

Cite this article as: Djoudi, O., Lalouni Belaid, S., Tamalouzt, S. "Multilevel Converter and Fuzzy Logic Solutions for Improving Direct Control Accuracy of DFIG-based Wind Energy System", Periodica Polytechnica Electrical Engineering and Computer Science, 67(2), pp. 136–148, 2023.
https://doi.org/10.3311/PPee.21047

done by PI controllers. However, the PWM block is still used and the control model depends on the system parameters. In [15], DC-link voltage variations have been minimized, nevertheless, variations of the grid parameters have an impact on the suggested control model. In [16], authors present a control technique, that combines the benefits of VOC and Virtual Flux DPC (VFDPC), based on the GSC active/reactive powers expressions. Yet, the use of an additional PI controller, compared to VFDPC, increases the sensitivity to parametric variations. In addition, the regulation of the GSC currents using hysteresis controllers, which impose a variable switching frequency and considerable ripples. On the other hand, several approaches for improving RSC performances have been proposed [17, 18]. Ayyarao [17] propose the enhancing of torque and flux performances by using sliding mode control (SMC). However, the chattering phenomenon is still encountered. In [18], the authors propose a fixed switching frequency control strategy. However, this control strategy based on PI controllers which is sensitive to DFIG parametric variations.

Nowadays, artificial intelligence is of great interest in the field of automation and industrial process control. In [19], torque and flux ripples were minimized by artificial neural network (ANN), but the control implementation is very tricky. A fuzzy logic controller (FLC) is a control strategy that emulates human reasoning, it has various advantages, such as inexpensive to develop, easy to grasp, and it can handle complex non-linear systems [20]. In [21, 22], a considerable improvement in flux and torque ripples were recorded in the DFIG by the DTC fuzzy switching table. Another possibility to improve the DFIG controls performances is to act on the power converter. The two-level converter is affected by several problems, among them low PWM switching frequency and high switching losses [23]. Moreover, the output voltage level is limited, which directly affects the system performances. The use of multilevel converters seems to be an interesting solution. Among them, the three-level (3L) converter is an appropriate solution in terms of performances and investment cost [24]. In [25], torque and flux ripples in the DFIG were mitigated thanks to the three-level inverter flexibility. The control techniques proposed in [21–23] show satisfactory performances, torque/flux ripples minimization with fast and accurate response, easy implementation and robustness against parametric variations. Nevertheless, the global wind energy conversion system control remains insufficient, because the GSC control is neglected.

The following are the paper's main contributions:

- A comparison between two methods allowing the DFIG performances improvement by acting on the type of the RSC converter or its control method (a three-level inverter controlled by a conventional DTC (3L-CDTC) versus to a two-level inverter controlled by a fuzzy DTC (2L-FDTC));
- DFIG continuous control in three distinct operating modes (synchronous, sub-synchronous and super-synchronous);
- The GSC controlled by a fuzzy switching table based DPC.

The rest of this paper is laid out as follows: Section 2 presents and models the WT-DFIG. Section 3 introduces the principle of conventional and enhanced DTC. Section 4 discusses how an improved DPC can control the GSC. Section 5 presents the simulation results performed on MATLAB/Simulink environment and discussions. Section 6 concludes the paper.

2 Modeling of the studied WT-DFIG system

Fig. 1 depicts the overall wind power conversion system for the DFIG driven by the conventional direct control (CDC) applied to three-level back-to-back converters. Fig. 2 illustrates the DFIG controlled using the direct control, enhanced with a fuzzy logic approach.

2.1 WT-DFIG modeling

The wind's kinetic energy is transformed into mechanical energy by the WT which is recovered from the rotating shaft. The mechanical power on the turbine shaft is expressed by Eq. (1):

$$P_t = \frac{1}{2} \cdot C_p(\lambda,\ \beta) \cdot \rho \cdot S \cdot v_v^3, \tag{1}$$

where C_p, ρ, S, and v_v are respectively power coefficient, air density, circular sweep of the turbine and wind speed. The power coefficient of the WT used is determined by Eq. (2):

$$C_p = 0.5 \cdot \sin\left(\pi(\lambda + 0.1)/18\right). \tag{2}$$

The slow turbine speed is adapted to the DFIG speed using a gearbox, as given by Eqs. (3) and (4) [26]:

$$\begin{cases} T_m = \dfrac{T_t}{G} \\ \Omega_m = \Omega_t \cdot G \end{cases}. \tag{3}$$

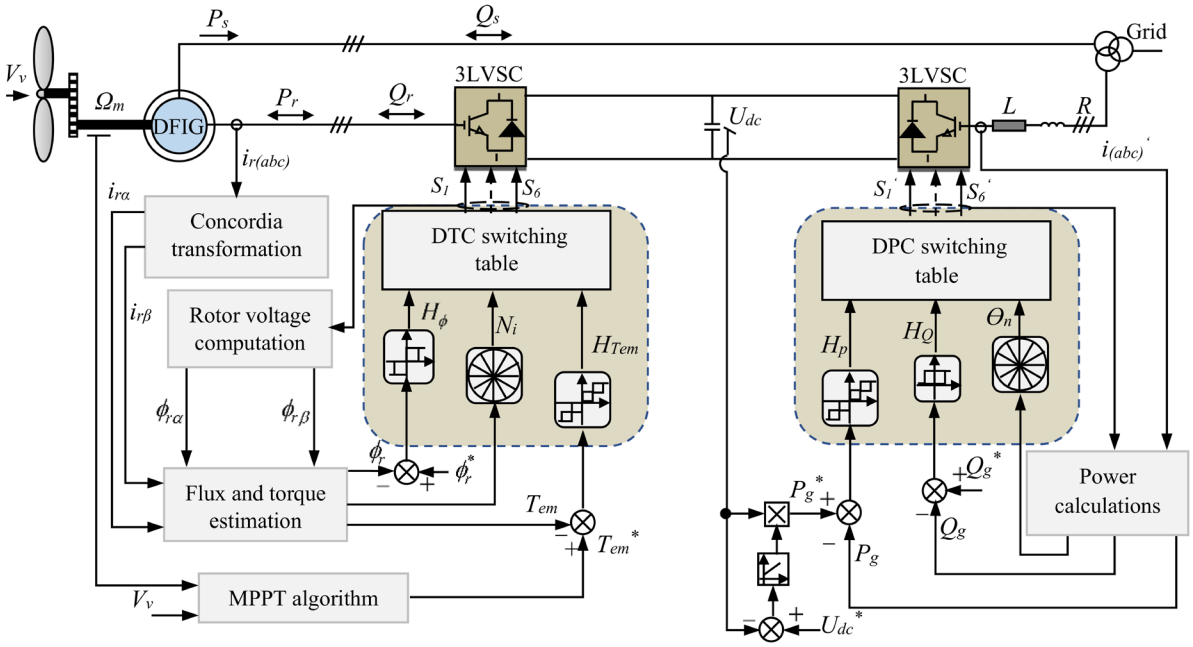

Fig. 1 Structure of WT-DFIG control by 3L-CDC

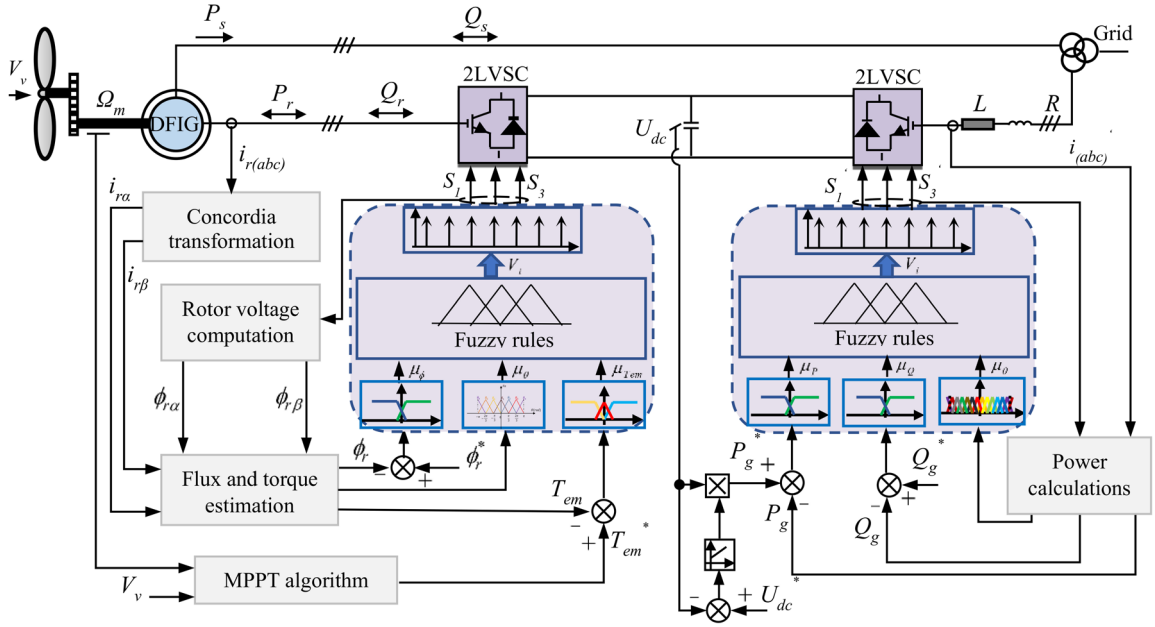

Fig. 2 Structure of WT-DFIG control by 2L-FDC

Equation (4) gives the wind turbine dynamic model, where J represents the system's total inertia and f_v represents the friction coefficient:

$$J\frac{d\Omega_m}{dt}+f_v\Omega_m=T_m-T_{em}. \tag{4}$$

The DFIG dynamic model in the d-q synchronous frame is described by Eq. (5) [27]:

$$\begin{cases} V_{sd}=R_s i_{sd}+\dfrac{d\phi_{sd}}{dt}-\omega_s\phi_{sq} \\ V_{sq}=R_s i_{sq}+\dfrac{d\phi_{sq}}{dt}+\omega_s\phi_{sd} \\ V_{rd}=R_r i_{rd}+\dfrac{d\phi_{rd}}{dt}-\omega_r\phi_{rq} \\ V_{rq}=R_r i_{rq}+\dfrac{d\phi_{rq}}{dt}+\omega_r\phi_{rd} \end{cases}, \tag{5}$$

where V_{sd}, V_{sq} and V_{rd}, V_{rq} are respectively d-q stator and rotor voltage components. i_{sd}, i_{sq} and i_{rd}, i_{rq} are respectively d-q stator and rotor current components. The stator and rotor electrical pulsations are respectively ω_s and ω_r. R_s, R_r are the stator/rotor phase resistances.

The DFIG magnetic flux equations as a function of stator/rotor current are given by Eq. (6):

$$\begin{cases} \phi_{sd} = L_s i_{sd} + M i_{rd} \\ \phi_{sq} = L_s i_{sq} + M i_{rq} \\ \phi_{rd} = L_r i_{rd} + M i_{sd} \\ \phi_{rq} = L_r i_{rq} + M i_{sq} \end{cases}, \tag{6}$$

where L_s and L_r are respectively the stator and rotor phase leakage inductances and M the mutual.

2.2 Algorithm for maximum operating of wind turbine

An optimal operating in WECS is very important. The MPPT algorithm enables to optimize the power extracted from the wind and thus to enhance the conversion efficiency [9]. The power coefficient C_p has a parabolic shape. It admits a maximum at the optimal speed ratio λ_{opt}, as presented in Fig. 3.

The MPPT algorithm generates the reference of electromagnetic torque; the speed ratio is kept at its optimum λ_{opt} and the power coefficient at its maximal value $C_{p-\max}$.

The electromagnetic torque reference is calculated as follows in Eq. (7) [28]:

$$T_{em-ref} = \frac{1}{2} \cdot C_{p-\max} \frac{\rho \cdot \pi \cdot R^5}{G^3 \cdot \lambda_{opt}^3} \cdot v_v^3. \tag{7}$$

3 DTC control of RSC

The DTC control is competitive with conventional methods [7], it allows direct control of DFIG's torque and flux.

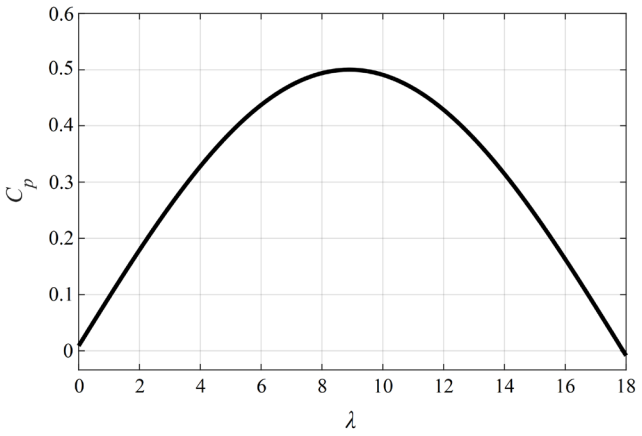

Fig. 3 $C_p(\lambda, \beta)$ characteristic for $\beta = 0°$

Its main principle is to select an appropriate voltage vector that compensates the rotor flux and electromagnetic torque errors, without their eventual measurement. Fig. 4 depicts an example of the voltage vectors selection when flux is positioned in the second sector.

The rotor flux magnitude is obtained using ($\phi_{r\alpha}$, $\phi_{r\beta}$) components, as follows in Eqs. (8) and (9) [21]:

$$\begin{cases} \phi_{r\alpha}(t) = \int_0^t \left(V_{r\alpha} - R_r i_{r\alpha}\right) dt \\ \phi_{r\beta}(t) = \int_0^t \left(V_{r\beta} - R_r i_{r\beta}\right) dt \end{cases}, \tag{8}$$

$$\phi_r = \sqrt{\phi_{r\alpha}^2 + \phi_{r\beta}^2}. \tag{9}$$

The rotor current components, the flux ($\phi_{r\alpha}$, $\phi_{r\beta}$), and pair pole number (p) can all be used to calculate the electromagnetic torque (Eq. (10)) [15]:

$$T_{em} = p\left(\phi_{r\alpha} i_{r\beta} - \phi_{r\beta} i_{r\alpha}\right). \tag{10}$$

The improvement of DTC performances is done by first acting on the inverter (DTC with three-level inverter), then the fuzzy logic concept is employed for the enhancement of the DTC control (FDTC with two-level inverter).

3.1 Conventional DTC with three-level inverter

Fig. 5 depicts the three-level NPC converter structure.

The voltage between phase and neutral can have three voltage levels, depending on the selection of the quarter switches of each leg. Two switches on each leg support half of the DC-link voltage, thus reducing voltage and power losses. In contrast to the two-level inverter, the entire DC-link voltage is supported by a single switch.

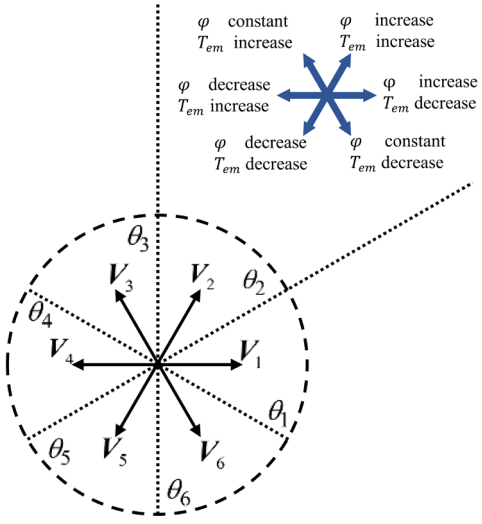

Fig. 4 Voltage vectors selection to compensate the flux and torque error

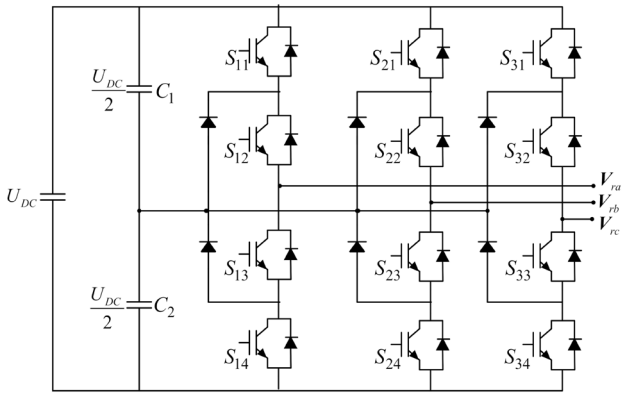

Fig. 5 Schema of three-level NPC inverter

The following matrix represents the three-level inverter mathematical model, where V_{ra}, V_{rb} and V_{rc} are the rotor phase voltage, U_{DC} represents the DC-link voltage and S_{ki} are the switching states of inverter (Eq. (11)):

$$\begin{bmatrix} V_{ra} \\ V_{rb} \\ V_{rc} \end{bmatrix} = \frac{U_{DC}}{3} \begin{bmatrix} 2 & -1 & -1 \\ -1 & 2 & -1 \\ -1 & -1 & 2 \end{bmatrix} \begin{bmatrix} S_{11}S_{12} - S_{13}S_{14} \\ S_{21}S_{22} - S_{23}S_{24} \\ S_{31}S_{32} - S_{33}S_{34} \end{bmatrix}. \tag{11}$$

The three-level converter advantages over the two-level one in DTC control is that its spatial representation of the voltage vectors has three hexagons, as shown in Fig. 6, which provides a large degree of freedom in DTC control of DFIG, which improves THD by lowering torque and flux ripples.

The rotor flux control is provided by a three-level hysteresis comparator (−1, 0, 1) this means decrease, keep constant and increase the flux respectively, while the electromagnetic torque control is provided by a five-level hysteresis comparator (−2, −1, 0, 1, 2), this means decrease more strongly, decrease less strongly, keep constant, increase less strongly and increase more strongly the torque respectively.

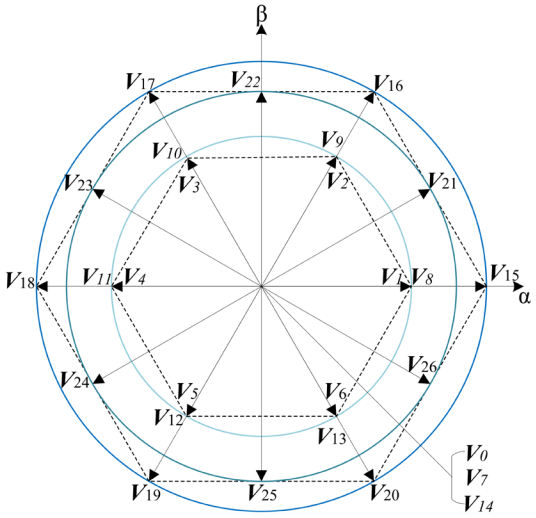

Fig. 6 Voltage vectors delivered by the three-level converter

The converter's switching vector is deduced by the states of the flux and electromagnetic torque controllers, including the rotor flux position, as shown in Table 1. The sector numbers are determined according to Eq. (12):

$$\frac{-\pi}{12} + (n-1)\frac{\pi}{6} \le N_n \le \frac{\pi}{12} + (n-1)\frac{\pi}{6}. \tag{12}$$

Table 1 Three-level inverter DTC switching table [26]

H_ϕ	H_{Tem}	Sectors											
		N_1	N_2	N_3	N_4	N_5	N_6	N_7	N_8	N_9	N_{10}	N_{11}	N_{12}
	+2	V_{21}	V_{16}	V_{22}	V_{17}	V_{23}	V_{18}	V_{24}	V_{19}	V_{25}	V_{20}	V_{26}	V_{15}
	+1	V_{21}	V_2	V_{22}	V_3	V_{23}	V_4	V_{24}	V_5	V_{25}	V_6	V_{26}	V_1
+1	0	Zero vector											
	−1	V_{26}	V_1	V_{21}	V_2	V_{22}	V_3	V_{23}	V_4	V_{24}	V_5	V_{25}	V_6
	−2	V_{26}	V_{15}	V_{21}	V_{16}	V_{22}	V_{17}	V_{23}	V_{18}	V_{24}	V_{19}	V_{25}	V_{20}
	+2	V_{22}	V_{17}	V_{23}	V_{18}	V_{24}	V_{19}	V_{25}	V_{20}	V_{26}	V_{15}	V_{21}	V_{16}
	+1	V_{22}	V_3	V_{23}	V_4	V_{24}	V_5	V_{25}	V_6	V_{26}	V_1	V_{21}	V_2
0	0	Zero vector											
	−1	V_{25}	V_6	V_{26}	V_1	V_{21}	V_2	V_{22}	V_3	V_{23}	V_4	V_{24}	V_5
	−2	V_{25}	V_{20}	V_{26}	V_{15}	V_{21}	V_{16}	V_{22}	V_{17}	V_{23}	V_{18}	V_{24}	V_{19}
	+2	V_{17}	V_{23}	V_{18}	V_{24}	V_{19}	V_{25}	V_{20}	V_{26}	V_{15}	V_{21}	V_{16}	V_{22}
	+1	V_3	V_{23}	V_4	V_{24}	V_5	V_{25}	V_6	V_{26}	V_1	V_{21}	V_2	V_{22}
−1	0	Zero vector											
	−1	V_5	V_{25}	V_6	V_{26}	V_1	V_{21}	V_2	V_{22}	V_3	V_{23}	V_4	V_{24}
	−2	V_{19}	V_{25}	V_{20}	V_{26}	V_{15}	V_{21}	V_{16}	V_{22}	V_{17}	V_{23}	V_{18}	V_{24}

3.2 Fuzzy DTC with two-level inverter

The analog input information of the hysteresis controller is coded into digital output. In other terms, the large amount of information that arrives is converted into a small number of decisions at the output of the hysteresis controller [22]. This means that the hysteresis controller loses information, its uses in DTC control results in a control performances degradation. This degradation is observed by the increase in flux and torque ripples due to the lack of accuracy of the strategy used. Fuzzy logic is an effective solution to this problem. Its principle is to assign to the input variable a degree of affiliation to the fuzzy sets and, from the fuzzy rules, the most efficient decision is selected [11].

Fig. 7 presents the fuzzy inputs. The torque error fuzzy input is made up of three linguistic variables (P: Positive, Z: Zero and N: Negative). Whereas the flux error fuzzy input consists of two linguistic variables (P: Positive and N: Negative). The rotor flux position is determined from the division of the frame into six fuzzy sectors according to Eq. (13):

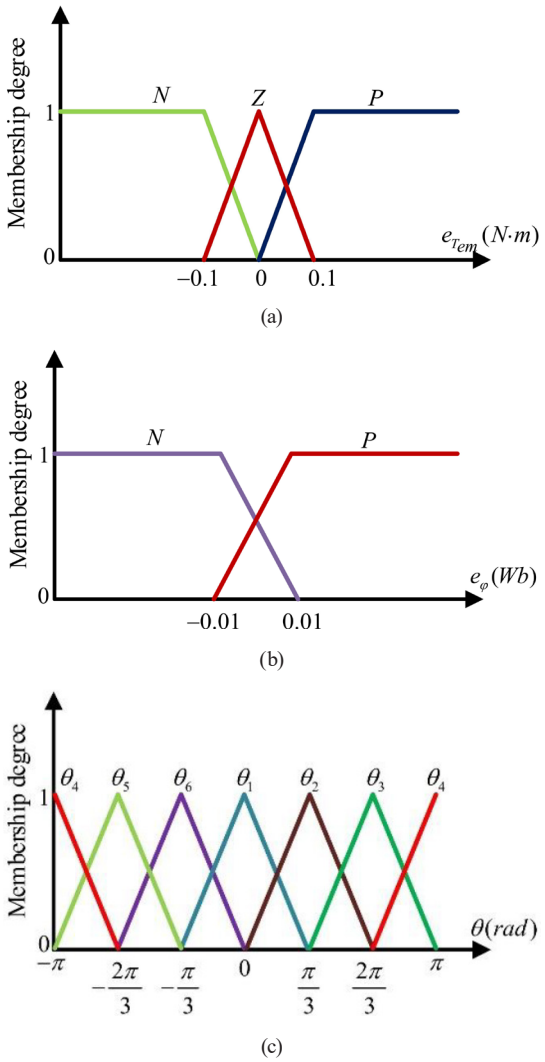

Fig. 7 Membership functions of the fuzzy inputs; (a) Torque error fuzzy membership functions; (b) Flux error fuzzy membership functions; (c) Flux position fuzzy membership functions

$$\left(2n-3\right)\frac{\pi}{6} \le \theta_n \le \left(2n-1\right)\frac{\pi}{6};\ \ n=1,2,...,6. \tag{13}$$

In this control method, the fuzzy controller output is the switching vector ($\boldsymbol{V}_0$–$\boldsymbol{V}_7$) to be used on the RSC. The fuzzy switching table has 36 fuzzy rules, as depicted in Table 2.

The inference process generates the fuzzy rules based on the state of the fuzzy inputs. The choice of the appropriate voltage vector is based on the Mamdani Min-Max method. The mathematical concept used by this method is given by Eqs. (14) to (16):

$$a_i = \min\left(\mu_{Xi}\left(e_{Tem}\right),\ \mu_{Yi}\left(e_{\varphi}\right),\ \mu_{Zi}\left(\theta\right)\right), \tag{14}$$

$$\mu_{Vi}^{'}\left(V\right) = \max\left(a_i,\ \mu_{Vi}\left(V\right)\right), \tag{15}$$

$$\mu_{Vout}\left(V\right) = \max_{i=1}^{36}\left(\mu_{Vi}^{'}\left(V\right)\right), \tag{16}$$

where $\mu_{Xi}(e_{Tem})$, $\mu_{Yi}(e_{\varphi})$ and $\mu_{Zi}(\theta)$ are the membership degree of the three fuzzy inputs of the FDTC [21]. The largest of the maximum (LOM) method is used for the defuzzification method chosen to give the numerical value of the output membership functions. The block diagram of the FLC is given by Fig. 8.

The results presented in Figs. 9 and 10 demonstrate the high efficiency of the 2L-FDTC control structure ahead of 3L-CDTC.

An improvement of torque/flux ripples is observed using the 3L-CDTC compared to the 2L-CDTC with 41.6% and 47.5% respectively. While the improvement obtained by the 2L-FDTC reached 85.71% for the electromagnetic torque and 66.6% for the rotor flux. It can also be seen that the system response is faster with a 2L-FDTC control.

Considering the comparison results between 3L-CDTC and 2L-FDTC, the 2L-FDPC is adopted for the control of the GSC.

Table 2 Fuzzy inference basis of FDTC

e_{ϕ}	e_{Tem}	Sectors					
		θ_1	θ_2	θ_3	θ_4	θ_5	θ_6
	P	V_2	V_3	V_4	V_5	V_6	V_1
P	Z	V_1	V_2	V_3	V_4	V_5	V_6
	N	V_6	V_1	V_2	V_3	V_4	V_5
	P	V_3	V_4	V_5	V_6	V_1	V_1
N	Z	V_0	V_7	V_0	V_7	V_0	V_7
	N	V_5	V_6	V_1	V_2	V_3	V_4

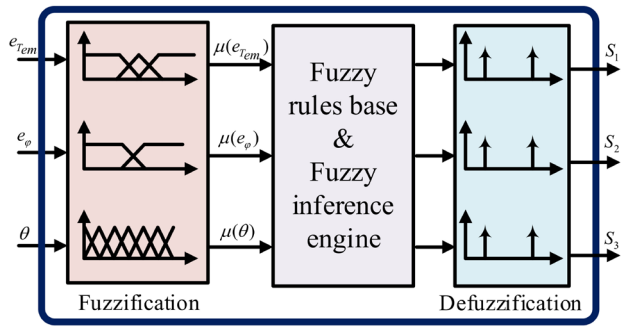

Fig. 8 2L-FDTC Block diagram

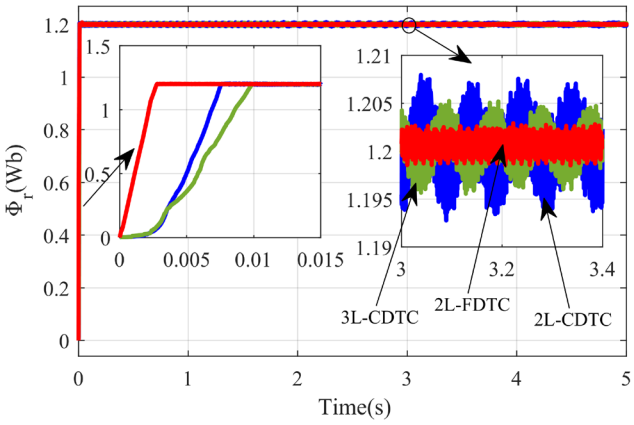

Fig. 9 Magnitude flux response

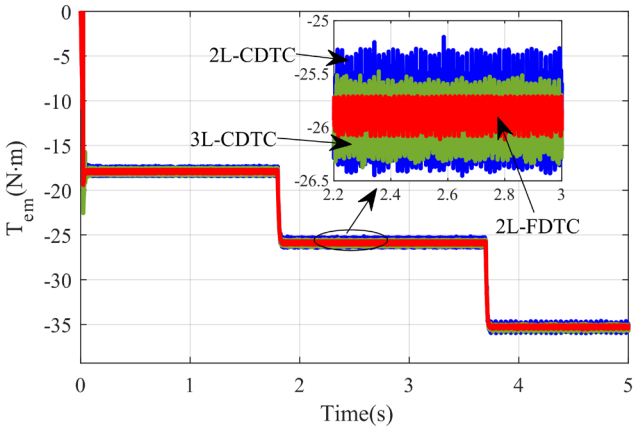

Fig. 10 Electromagnetic torque response

4 DPC control of GSC

The DPC applied to the GSC allows direct and instantaneous control of active/reactive exchanged powers between the generator's rotor and the AC grid [29]. Using hysteresis comparators, the errors between the references and measured values of the active/reactive powers were digitalized, as well as the grid voltage angular location, are used to determine the optimal voltage vectors. Controlling the DC-link voltage with a PI controller provides the active power reference, setting the reference reactive power to zero results in the unit power factor. According to Eq. (17), the active/reactive powers may be determined from the grid voltage and current [30, 31]:

$$\begin{cases} P = V_{G\alpha} i_{\alpha}^{'} + V_{G\beta} i_{\beta}^{'} \\ Q = V_{G\alpha} i_{\beta}^{'} - V_{G\beta} i_{\alpha}^{'} \end{cases}. \tag{17}$$

The knowledge of the grid voltage vector position is required for the selection of adequate switching states. It is determined using Eq. (18):

$$\theta = \tan^{-1} \frac{V_{G\beta}}{V_{G\alpha}}. \tag{18}$$

Equation (19) is used to compute the sector position:

$$(n-2)\frac{\pi}{6} \le \sigma_n \le (n-1)\frac{\pi}{6};\ n = 1,2,...,12. \tag{19}$$

Table 3 illustrates the optimal voltage vector selection based on the grid voltage vector location and the status of the active/reactive powers hysteresis controllers.

4.1 Fuzzy DPC for GSC

By eliminating the hysteresis controllers, the fuzzy DPC aims to minimize the active/reactive powers ripples that exist in two-level DPC [29].

As in the conventional DPC switching table, the active/reactive powers errors and the voltage vector position, constitute the fuzzy inputs. The powers are characterized by two membership functions:

- *P*: when the power reference is greater than the estimated value;
- *N*: when the estimated power is higher than the reference one.

The grid voltage angular position is divided into 12 fuzzy sectors (Fig. 11).

The defuzzification is obtained by the LOM method in order to guarantee a binary type output. Therefore, the fuzzy output is determined from 48 fuzzy rules, as is indicated in Table 4.

As in FDTC, the control rules in the FDPC are given by the Mamdani Min-Max method. The output voltage vector is determined according to Eqs. (20) to (22):

Table 3 DPC switching table [30]

H_p	H_q	σ_1	σ_2	σ_3	σ_4	σ_5	σ_6	σ_7	σ_8	σ_9	σ_{10}	σ_{11}	σ_{12}
−1	1	V_6	V_1	V_1	V_2	V_2	V_3	V_3	V_4	V_4	V_5	V_5	V_6
	−1	V_1	V_2	V_2	V_3	V_3	V_4	V_4	V_5	V_5	V_6	V_6	V_1
1	1	V_7	V_7	V_0	V_0	V_7	V_7	V_0	V_0	V_7	V_7	V_0	V_0
	−1	V_6	V_7	V_1	V_0	V_2	V_7	V_3	V_0	V_4	V_7	V_5	V_0

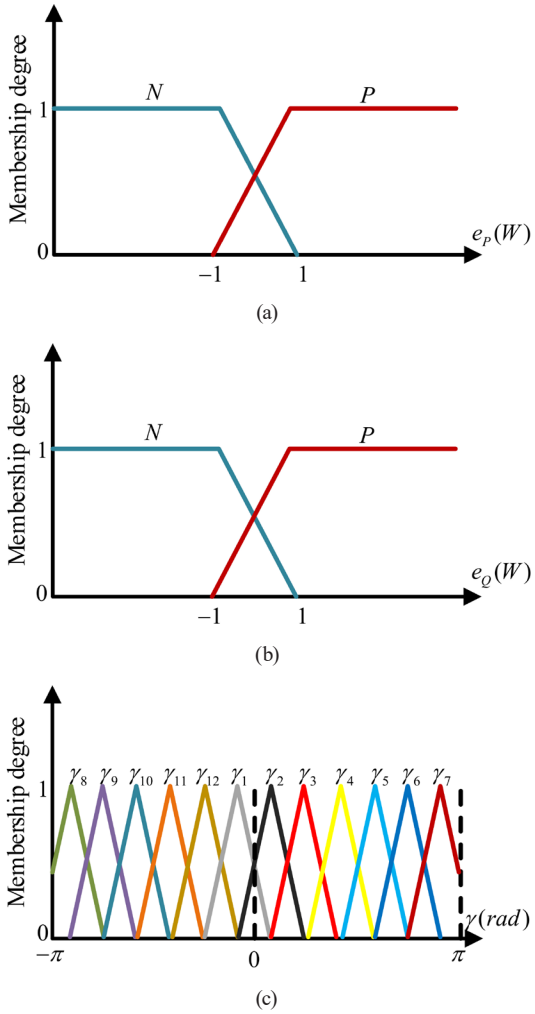

Fig. 11 Membership functions of the GSC-DPC fuzzy inputs; (a) Fuzzy membership functions of GSC active power; (b) Fuzzy membership functions of GSC reactive power; (c) Fuzzy membership functions of grid voltage angular position

Table 4 Fuzzy DPC switching table [31]

e_p	e_q	γ_1	γ_2	γ_3	γ_4	γ_5	γ_6	γ_7	γ_8	γ_9	γ_{10}	γ_{11}	γ_{12}
N	P	V_6	V_1	V_1	V_2	V_2	V_3	V_3	V_4	V_4	V_5	V_5	V_6
	N	V_1	V_2	V_2	V_3	V_3	V_4	V_4	V_5	V_5	V_6	V_6	V_1
P	P	V_7	V_7	V_0	V_0	V_7	V_7	V_0	V_0	V_7	V_7	V_0	V_0
	N	V_6	V_7	V_1	V_0	V_2	V_7	V_3	V_0	V_4	V_7	V_5	V_0

$$a_i = \min\left(\mu_{Xi}(e_P),\ \mu_{Yi}(e_Q),\ \mu_{Zi}(\gamma)\right), \tag{20}$$

$$\mu'_{Vi}(V) = \max\left(a_i, \mu_{Vi}(V)\right), \tag{21}$$

$$\mu_{Vout}(V) = \max_{i=1}^{48}\left(\mu'_{Vi}(V)\right), \tag{22}$$

where $\mu_{Xi}(e_P)$, $\mu_{Yi}(e_Q)$ and $\mu_{Zi}(\gamma)$ are the membership degree of the three fuzzy inputs of the FDPC [21].

5 Simulation results

A MATLAB/Simulink simulation has been performed to test the efficiency of the suggested control. Tables A1 and A2 in Appendix show the parameters used for the studied system [32]. The variable wind speed displayed in Fig. 12 has been carefully fixed to run the DFIG in all operating modes (sub-synchronous, synchronous and super-synchronous) and the MPPT region.

Figs. 13 to 17 show respectively the evolution of the rotor flux, electromagnetic torque, DC-link voltage and GSC active/reactive powers, for the two controllers (2L-CDC and 2L-FDC).

By analyzing the results obtained after zooming, we can see that the 2L-FDC control structure has better performances; where, the ripples have been considerably minimized compared to the 2L-CDC structure, 75% for the torque, 65% for the rotor flux. In addition, 52% and 50% of improvement are observed for the GSC active and reactive powers.

The DC-link voltage response tracks its reference value of 660V for both control strategies. When the 2L-FDC structure is implemented, reaches its reference with small overshoot.

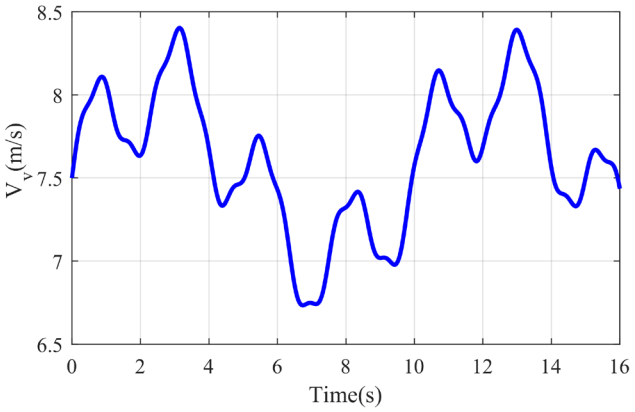

Fig. 12 Wind speed profile

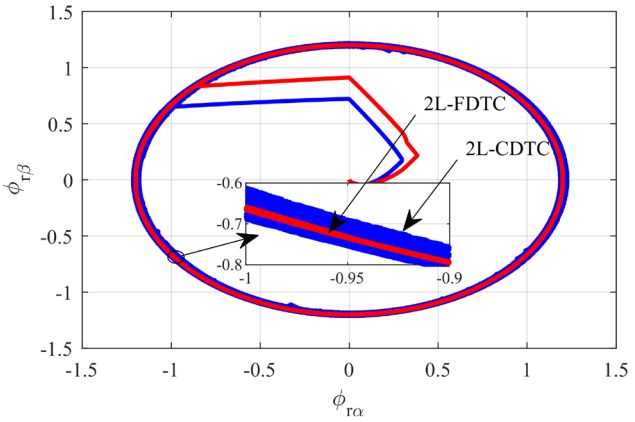

Fig. 13 Rotor flux with zoom

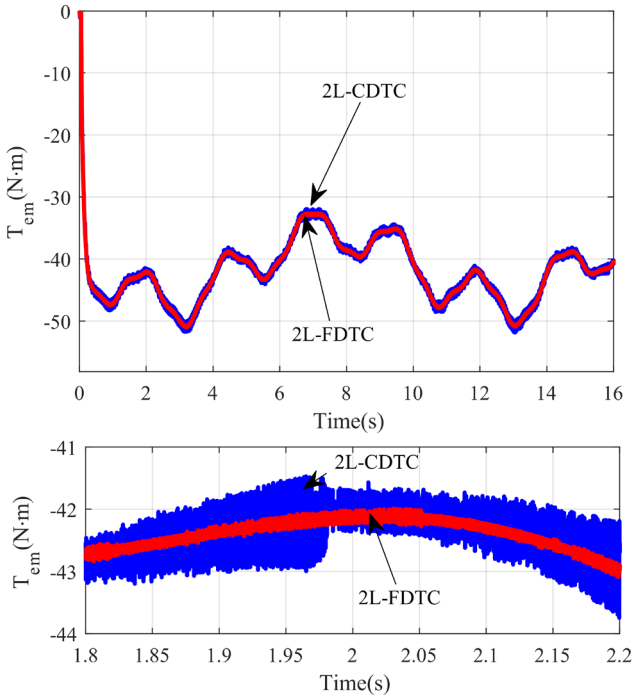

Fig. 14 Electromagnetic torque response with its zoom

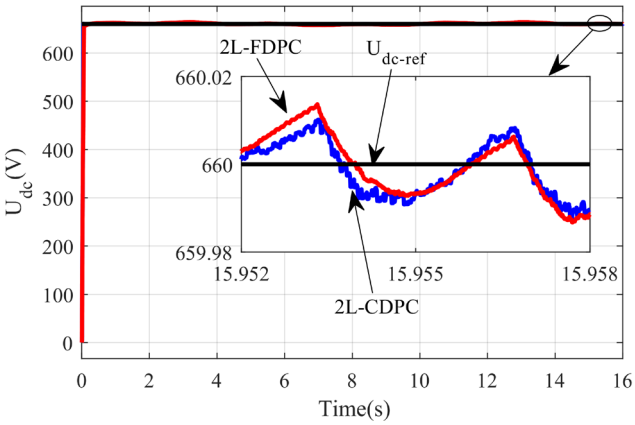

Fig. 15 DC-link voltage with its reference

Figs. 18 to 23 show the results obtained with the 2L-FDC control strategy. The DFIG operating modes can be found thanks to its slip which is represented by Fig. 18; it's positive in sub-synchronous mode, zero in synchronous mode and negative in super-synchronous operation mode. The DFIG reference speed is obtained from the MPPT algorithm. The speed ratio and power coefficient are at their optimal values (Fig. 19).

The stator current waveform is shown in Fig. 21. Since the stator is connected directly to the grid, the stator current frequency is always equal to the grid frequency. On the opposite, the rotor current frequency varies according to the slip since the stator frequency is kept constant (Fig. 22).

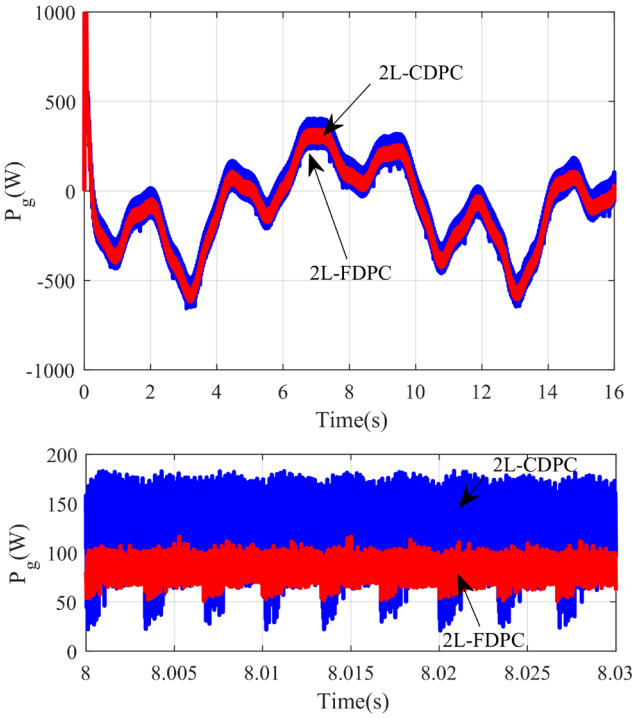

Fig. 16 Waveform of active power delivered by the GSC with its zoom

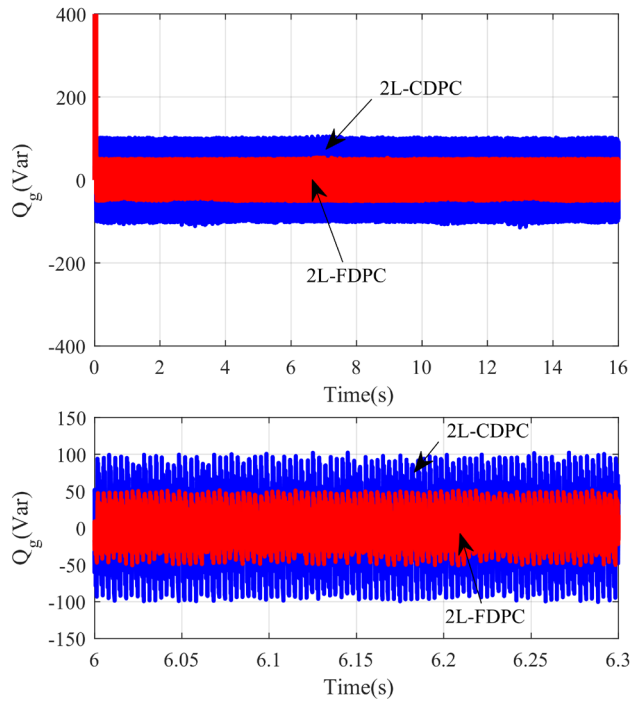

Fig. 17 Waveform of reactive power delivered by the GSC with its zoom

The active stator/rotor powers are depicted in Fig. 23. The stator active power always remains negative during the three operation modes, the DFIG supplies active power to grid through the stator.

The rotor and the grid exchange active power in both directions. During the sub-synchronous mode, the rotor

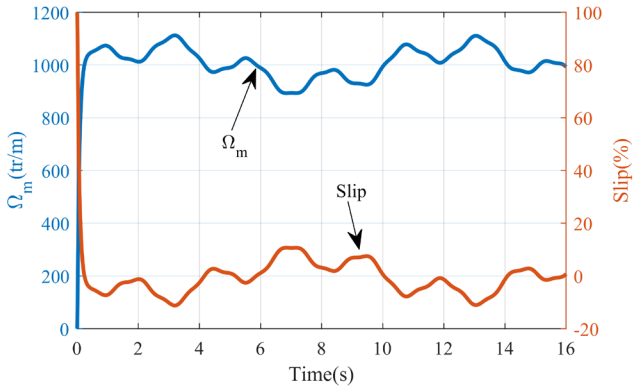

Fig. 18 Mechanical DFIG speed and slip

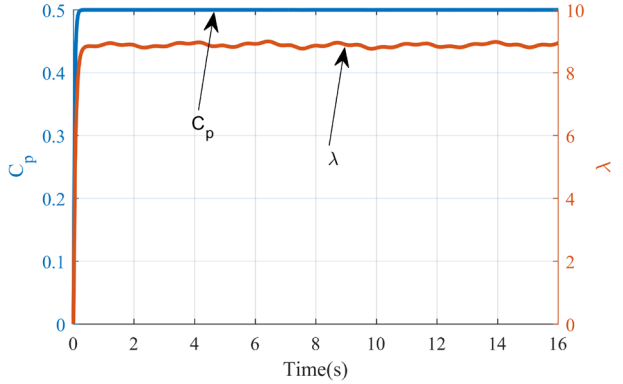

Fig. 19 Waveforms of power coefficient and speed ratio

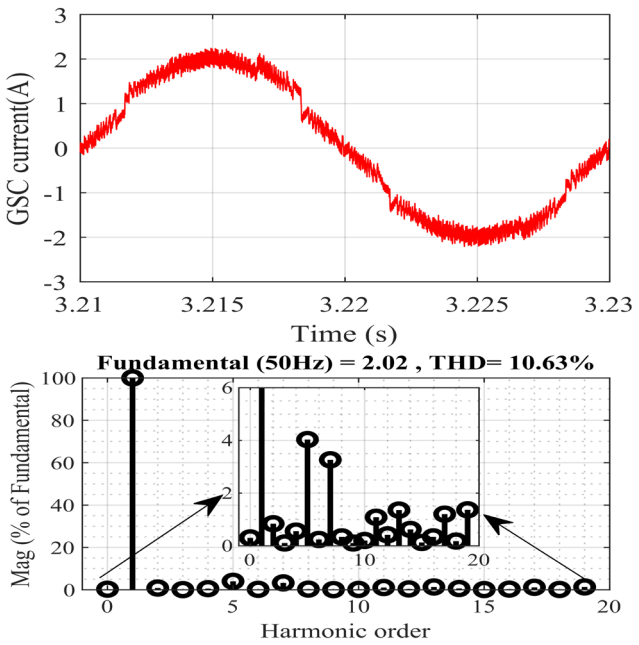

(a)

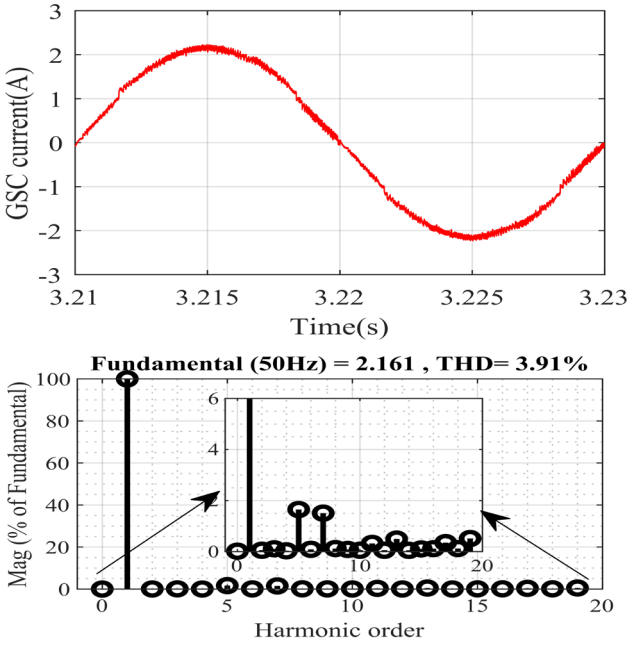

(b)

Fig. 20 Waveforms of generated GSC current with its harmonic spectrum; (a) 2L-CDC; (b) 2L-FDC

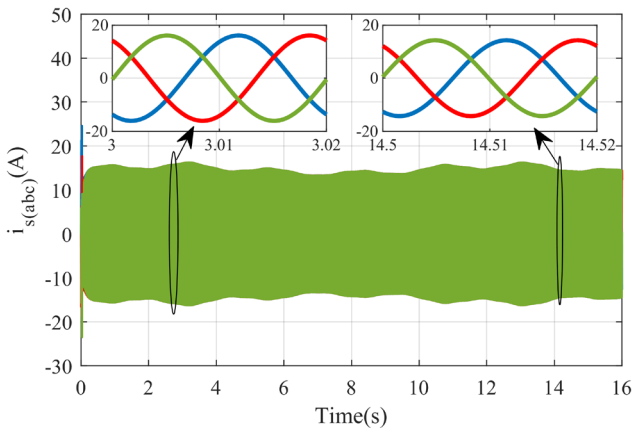

Fig. 21 Evolution of stator current

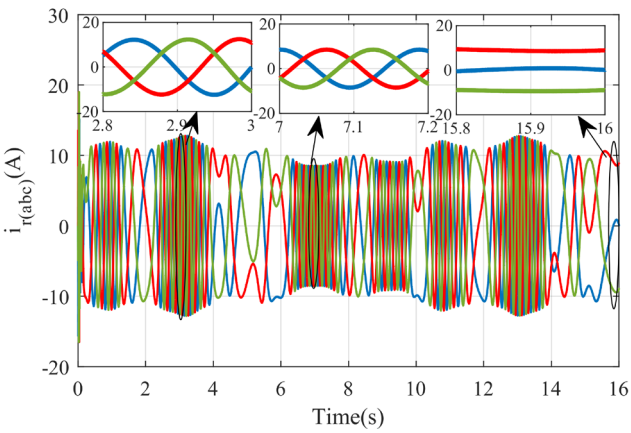

Fig. 22 Evolution of rotor current

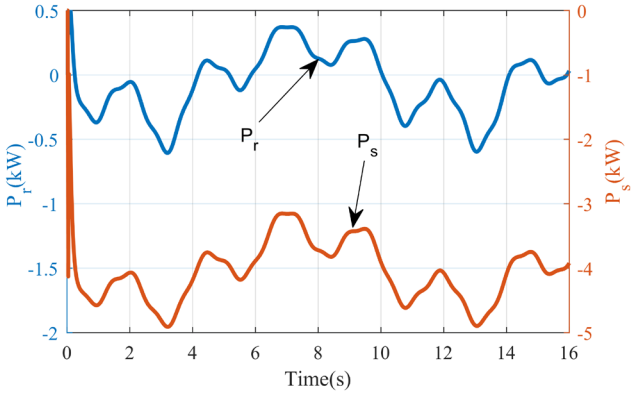

Fig. 23 Waveforms of stator and rotor active power

active power is positive; then the grid that supplies the DFIG rotor. An improvement of the grid current THD of 63% is observed during operation in Super-synchronous mode when the GSC is controlled using the proposed fuzzy DPC compared to the conventional DPC, as shown in Fig. 20.

6 Conclusion

This paper proposes two appropriate solutions to overcome the ripples problem often encountered in DTC and DPC controls applied to two-level converters for DFIG control of grid-connected WECS. The first solution is to increase the level of hysteresis controllers by means of a large number of voltage vectors at the output of three-level converters. The usual switching table has been replaced by fuzzy rules in the second solution. The results of the proposed method 2L-FDTC shows highest efficiency against the 3L-CDTC method. The simulation results of the DFIG-based 2L-FDC control under variable wind speed demonstrated significant ripples minimization, more than 65% in both torque and flux, and a reduction of over 50% in power ripples is achieved compared to the 2L-CDC is achieved compared to 2L-CDC. Furthermore, the 2L-FDPC allows an optimal and high dynamic power generation with low THD.

References

[1] Jung, C., Taubert, D., Schindler, D. "The temporal variability of global wind energy – Long-term trends and inter-annual variability", Energy Conversion and Management, 188, pp. 462–472, 2019. https://doi.org/10.1016/j.enconman.2019.03.072

[2] Rani, P., Arora, V. P., Sharma, N. K. "Improved dynamic performance of permanent magnet synchronous generator based grid connected wind energy system", Energy Sources, Part A: Recovery, Utilization, and Environmental Effects, 2022. https://doi.org/10.1080/15567036.2021.2022814

[3] Nugent, D., Sovacool, B. K. "Assessing the lifecycle greenhouse gas emissions from solar PV and wind energy: A critical meta-survey", Energy Policy, 65, pp. 229–244, 2014. https://doi.org/10.1016/j.enpol.2013.10.048

[4] Dekali, Z., Baghli, L., Boumediene, A. "Improved Super Twisting Based High Order Direct Power Sliding Mode Control of a Connected DFIG Variable Speed Wind Turbine", Periodica Polytechnica Electrical Engineering and Computer Science, 65(4), pp. 352–372, 2021. https://doi.org/10.3311/PPee.17989

[5] Djoudi, O., Lalouni Belaid, S., Tamalouzt, S. "A high degree of direct torque control applied to a grid-connected wind energy system based on a DFIG", Journal of Renewable Energies, 1(1), pp. 81–91, 2022. https://doi.org/10.54966/jreen.v1i1.1042

[6] Bossoufi, B., Karim, M., Lagrioui, A., Taoussi, M., Elhafyani, M. L. "Backstepping control of DFIG generators for wide-range variable-speed wind turbines", International Journal of Automation and Control, 8(2), pp. 122–140, 2014. https://doi.org/10.1504/IJAAC.2014.063359

[7] Moati, Y., Kouzi, K. "Investigating the Performances of Direct Torque and Flux Control for Dual Stator Induction Motor with Direct and Indirect Matrix Converter", Periodica Polytechnica Electrical Engineering and Computer Science, 64(1), pp. 97–105, 2020. https://doi.org/10.3311/PPee.14977

[8] Djoudi, A., Bacha, S., Iman-Eini, H. "Efficient real-time estimation for DFIG-Performance and reliability enhancement of grid/microgrid connected energy conversion systems", Journal of Renewable and Sustainable Energy, 11(2), 025503, 2019. https://doi.org/10.1063/1.5058076

[9] Hu, J., Yuan, X. "VSC-based direct torque and reactive power control of double fed induction generator", Renewable Energy, 40(1), pp. 13–23, 2012. https://doi.org/10.1016/j.renene.2011.08.023

[10] Ceballos, S., Rea, J., Lopez, I., Pou, J., Robles, E., O'Sullivan, D. L. "Efficiency Optimization in Low Inertia Wells Turbine-Oscillating Water Column Devices", IEEE Transactions on Energy Conversion, 28(3), pp. 553–564, 2013. https://doi.org/10.1109/TEC.2013.2265172

[11] Kouadria, S., Berkouk, E. M., Messlem, Y., Denaï, M. "Improved control strategy of DFIG-based wind turbine using direct torque and direct power control techniques", Journal of Renewable and Sustainable Energy, 10(4), 043306, 2018. https://doi.org/10.1063/1.5023739

[12] El Ouanjili, N., Derouich, A., Chebabhi, A., Taoussi, M. "A comparative study between FOC and DTC control of the Double Fed Induction Motor (DFIM)", In: 2017 International Conference on Electrical and Information Technologies (ICEIT), Rabat, Morocco, 2017, pp. 1–6. ISBN 978-1-5386-1517-1 https://doi.org/10.1109/EITech.2017.8255302

[13] Sahri, Y., Tamalouzt, S., Belaid Lalouni, S. "Enhanced Direct Power Control Strategy of a DFIG-Based Wind Energy Conversion System Operating Under Random Conditions", Periodica Polytechnica Electrical Engineering and Computer Science, 65(3), pp. 196–206, 2021. https://doi.org/10.3311/PPee.16656

[14] Gao, S., Zhao, H., Gui, Y., Zhou, D., Blaabjerg, F. "An Improved Direct Power Control for Doubly Fed Induction Generator", IEEE Transactions on Power Electronics, 36(4), pp. 4672–4685, 2021. https://doi.org/10.1109/TPEL.2020.3024620

[15] Zarei, M. E., Nicolás, C. V., Arribas, J. R., Ramírez, D. "Four-Switch Three-Phase Operation of Grid-Side Converter of Doubly Fed Induction Generator with Three Vectors Predictive Direct Power Control Strategy", IEEE Transactions on Industrial Electronics, 66(10), pp. 7741–7752, 2019. https://doi.org/10.1109/TIE.2018.2880672

[16] Mohammadi, J., Vaez-Zadeh, S., Ebrahimzadeh, E., Blaabjerg, F. "Combined control method for grid-side converter of doubly fed induction generator-based wind energy conversion systems", IET Renewable Power Generation, 12(8), pp. 943–952, 2018. https://doi.org/10.1049/iet-rpg.2017.0539

[17] Ayyarao, T. S. L. V. "Modified vector controlled DFIG wind energy system based on barrier function adaptive sliding mode control", Protection and Control of Modern Power Systems, 4(1), 4, 2019. https://doi.org/10.1186/s41601-019-0119-3

[18] Gupta, R., Dynamina, G. "Matlab Simulation of DTC-SVM of Doubly Fed Induction Generator for Wind Energy System", In: 2019 Innovations in Power and Advanced Computing Technologies (i-PACT), Vellore, India, 2019, pp. 1–6. ISBN 978-1-5386-8191-6 https://doi.org/10.1109/i-PACT44901.2019.8959990

[19] Benbouhenni, H., Boudjema, Z. "Two-level DTC based on ANN controller of DFIG using 7-level hysteresis command to reduce flux ripple comparing with traditional command", In: 2018 International Conference on Applied Smart Systems (ICASS), Medea, Algeria, 2018, pp. 1–8. ISBN 978-1-5386-6867-2 https://doi.org/10.1109/ICASS.2018.8652013

[20] Lalouni, S., Rekioua, D., Idjdarene, K., Tounzi, A. "Maximum Power Point Tracking Based Hybrid Hill-climb Search Method Applied to Wind Energy Conversion System", Electric Power Components and Systems, 43(8–10), pp. 1028–1038, 2015. https://doi.org/10.1080/15325008.2014.999143

[21] Ayrir, W., Haddi, A. "Fuzzy 12 sectors improved direct torque control of a DFIG with stator power factor control strategy", International Transactions on Electrical Energy Systems, 29(10), e12092, 2019. https://doi.org/10.1002/2050-7038.12092

[22] Sahri, Y., Tamalouzt, S., Lalouni Belaid, S., Bacha, S., Ullah, N., Al Ahamdi, A. A., Alzaed, A. N. "Advanced Fuzzy 12 DTC Control of Doubly Fed Induction Generator for Optimal Power Extraction in Wind Turbine System under Random Wind Conditions", Sustainability, 13(21), 11593, 2021. https://doi.org/10.3390/su132111593

[23] El Ouanjli, N., Derouich, A., El Ghzizal, A., Taoussi, M., El Mourabit, Y., Mezioui, K., Bossoufi, B. "Direct torque control of doubly fed induction motor using three-level NPC inverter", Protection and Control of Modern Power Systems, 4(1), 17, 2019. https://doi.org/10.1186/s41601-019-0131-7

[24] Noui, S., Tabbache, B., Hadjou, F., Berkouk, E.-M., Zhou, Z., Benbouzid. M. "Shoot-Through Control-Based Space Vector Modulation Approach for a Modified Z-Source NPC Power Inverter", Advances in Electrical and Electronic Engineering, 17(4), pp. 395–404, 2019. https://doi.org/10.15598/aeee.v17i4.3514

[25] Tamalouzt, S., Belkhier, Y., Sahri, Y., Bajaj, M., Ullah, N., Chowdhury, M. S., Titseesang, T., Techato, K. "Enhanced Direct Reactive Power Control-Based Multi-Level Inverter for DFIG Wind System under Variable Speeds", Sustainability, 13(16), 9060, 2021. https://doi.org/10.3390/su13169060

[26] Bakouri, A., Mahmoudi, H., Abbou, A., Moutchou, M. "Optimizing the wind power capture by using DTC technique based on Artificial Neural Network for a DFIG variable speed wind turbine", In: 2015 10th International Conference on Intelligent Systems: Theories and Applications (SITA), Rabat, Morocco, 2015, pp. 1–7. ISBN 978-1-5090-0220-7 https://doi.org/10.1109/SITA.2015.7358425

[27] Tamalouzt, S., Benyahia, N., Said Mohamed, M., Scipioni, A., Davat, B. "Direct Torque Control Applied to DFIG Supplied via a Three-Level Inverter Under Random Behavior Wind Speed", In: ELECTRIMACS 2019, Salerno, Italy, 2020, pp. 87–96. ISBN 978-3-030-37160-9 https://doi.org/10.1007/978-3-030-37161-6_7

[28] Narimene, K., Kheira, M., Mohamed, F. "Robust Neural Control of Wind Turbine Based Doubly Fed Induction Generator and NPC Three Level Inverter", Periodica Polytechnica Electrical Engineering and Computer Science, 66(2), pp. 191–204, 2022. https://doi.org/10.3311/PPee.19921

[29] Kahia, B., Bouafia, A., Chaoui, A., Zhang, Z., Abdelrahem, M., Kennel, R. "A direct power control strategy for three level neutral-point-clamped rectifier under unbalanced grid voltage", Electric Power Systems Research, 161, pp. 103–113, 2018. https://doi.org/10.1016/j.epsr.2018.04.010

[30] Ouchen, S., Betka, A., Gaubert, J. P., Abdeddaim, S. "Simulation and practical implementation of direct power control applied on PWM rectifier", In: 2017 6th International Conference on Systems and Control (ICSC), Batna, Algeria, 2017, pp. 567–571. ISBN 978-1-5090-3961-6 https://doi.org/10.1109/ICoSC.2017.7958748

[31] Lalouni Belaid, S., Boudries, Z., Aoumer, A. "Direct Power Control Improvement Using Fuzzy Switching Table of Grid Connected PV System", In: ICREEC 2019, Oran, Algeria, 2020, pp. 85–92. ISBN 978-981-15-5444-8 https://doi.org/10.1007/978-981-15-5444-5_11

[32] Pena, R., Cardenas, R., Escobar, E., Clare, J., Wheeler, P. "Control strategy for a Doubly-Fed Induction Generator feeding an unbalanced grid or stand-alone load", Electric Power Systems Research, 79(2), pp. 355–364, 2009. https://doi.org/10.1016/j.epsr.2008.07.005

Appendix

Table A1 DFIG parameters [32]

Parameter	Value
Rated power (kW)	7.5
Stator resistor (Ω)	1.06
Rotor resistor (Ω)	0.8
Stotor inductance (H)	0.093
Rotor inductance (H)	0.081
Mutuel inductance (H)	0.0664
Pairs poles number	3
Inertia moment (kg m²)	0.075

Table A2 Wind turbine parameters [32]

Parameter	Value
Rated power (kW)	7.5
Blade radius (m)	3.24
Gear box	5.065